Research Article Vol. 31, No. 21 / 9 Oct 2023 / Optics Express 34477
Optics EXPRESS

Design of low polarization off-axis three-mirror reflective optical systems

JING LUO,[1,*] TIANXIAO XU,[1,2] CHENGXU YOU,[1] YICHEN LIU,[1] CHENGHAO LI,[1] XIAOHUI ZHANG,[1] AND JIHONG DONG[1]

[1] *Chinese Academy of Science, Changchun Institute of Optics, Fine Mechanics and Physics, Changchun, Jilin 130033, China*
[2] *University of Chinese Academy of Sciences, Beijing 100049, China*
[*] *luojingopt@ciomp.ac.cn*

Abstract: Off-axis optical systems have several important advantages over on-axis ones. However, high polarization aberrations, which play important roles in many applications, become critical disadvantages of off-axis systems. Thanks to the seven free design parameters, three-mirror reflective systems have a good potential to achieve low polarization. A general method to design low polarization off-axis three-mirror reflective optical systems is proposed in this paper. Based on genetic algorithms, several off-axis three-mirror systems with both low polarization aberrations and good wave aberrations are designed. The method proposed in this paper is versatile and can be used to design other types of optical systems that demand low polarization aberrations.

1. Introduction

Thanks to several critical advantages such as wide diffraction-limited field of view (FOV), good ability to control stray light and stray heat, real exit pupil and compact structure design, three-mirror reflective optical systems [1,2] become competent candidates in astronomical observations [3–6], space investigation camera [7,8], remote sensing [9], and so on.

Polarization aberrations indicate the variations of amplitude, phase and polarization associated with rays passing through optical systems [10]. Comparing with wave aberrations, the impacts of polarization aberrations on imaging quality are so small that they can be ignored safely in many optical systems. However, for applications that demand ultra-high imaging quality or detection accuracy such as photolithographic imaging [11], polarimeter measurements [12], astronomical remote sensing [13–16] and coronagraphs [17], polarization aberrations become important error sources.

In our previous paper [18], it is the first time to confirm that on-axis three-mirror optical systems can simultaneously achieve good wave aberrations and low polarization aberrations. After low polarization optimization based on the method we proposed, polarization aberrations are reduced significantly and wave aberrations keep at a level that can achieve good image quality. As the results shown in our another paper [19], polarization aberrations of on-axis three-mirror systems are usually smaller than those of off-axis ones. Hence, it would be more necessary to reduce polarization aberrations for off-axis three-mirror optical systems.

In fact, off-axis systems have several important advantages over on-axis ones, such as simpler PSFs, easy stray light control, low-scattering property, larger throughput, and so on [20–22]. HabEx space telescope [23], SPICES [24], WFIRST-A [25], high-resolution imaging camera (HiRIC) [26] and CSST [5] belong to off-axis systems. Daniel K. Inouye solar telescope (DKIST), whose aperture is 4 m, is the largest optical solar telescope in the world [27]. Off-axis design is chosen by DKIST due to the advantages in thermal control and scattered light suppression, which are critical to solar observations [28]. In order to realize these advantages, however, a

#500651 https://doi.org/10.1364/OE.500651
Journal © 2023 Received 21 Jul 2023; revised 15 Sep 2023; accepted 15 Sep 2023; published 29 Sep 2023

Optics EXPRESS

number of technology challenges have to be overcome. The increase of polarization aberrations is one of the most important problems.

What is more, off-axis systems are even abandoned due to the drawback of high polarization aberrations. LUVOIR is a next generation space telescope proposed by NASA with the primary mission of detecting and characterizing planetary systems around nearby stars [29]. To achieve better high-contrast imaging performance, a lot of research has been done to choose an optimal telescope scheme for LUVOIR [30]. On-axis three-mirror telescopes and off-axis ones are two strong candidates. Their own advantages and disadvantages in many ways are compared carefully. Polarization aberrations have important impacts on coronagraph contrast so that it becomes one of the critical disadvantages of off-axis scheme to LUVOIR priorities [30]. If off-axis systems enable to achieve low polarization aberrations, the critical shortcoming is overcome and big advantages are established over on-axis ones. Hence, it is very necessary to reduce polarization aberrations of off-axis three-mirror systems through optical design.

In this paper, we are devoted to design low polarization aberrations off-axis three-mirror systems. The rest of this paper is arranged as follows. Basic design methods are shown in Section 2. In Section 3, several typical design results and examples are provided. The relationship between off-axis distance and polarization aberrations are discussed in Section 4. Some conclusions are summarized in Section 5.

2. Design method

Design of low polarization off-axis three-mirror reflective optical systems mainly consists of three parts: design of three-mirror systems with good wave aberrations, automatic obscuration elimination and low polarization systems realization. In this section, the three parts will be introduced in sequence.

2.1. Design of three-mirror systems with good wave aberrations

Three-mirror reflective optical systems are composed of three mirrors: a primary mirror (PM), a secondary mirror (SM) and a tertiary mirror (TM). For three-mirror systems, there are seven free design parameters, i.e., K_1, K_2, K_3, α_1, α_2, β_1 and β_2. K_1, K_2 and K_3 are the conic coefficients of PM, SM and TM, respectively. α_1 is the obscure ratio of SM to PM, α_2 is the obscure ratio TM to SM. β_1 and β_2 are the magnifications of SM and TM, respectively [31]. Assuming that the focal length of a three-mirror system is f', based on the definition of magnification and obscure ratio, the expressions for the radius of curvature of different mirrors r_i and their corresponding separations d_i can be calculated according to the paraxial optical theory [32]:

$$\begin{cases} r_1 = \frac{2f'}{\beta_1\beta_2} \\ r_2 = \frac{2\alpha_1 f'}{(1+\beta_1)\beta_2} \\ r_3 = \frac{2\alpha_1\alpha_2 f'}{1+\beta_2} \end{cases} \tag{1}$$

and

$$\begin{cases} d_1 = \frac{1-\alpha_1}{\beta_1\beta_2} f' \\ d_2 = \frac{\alpha_1(1-\alpha_2)f'}{\beta_2} \\ d_3 = \alpha_1\alpha_2 f' \end{cases} . \tag{2}$$

For most imaging applications, wave aberrations are far more important than polarization aberrations. Before realizing low polarization systems, hence, good wavefront performance must be achieved firstly. The relation between the third-order wave aberrations and the seven design parameters can be obtained by tracing marginal rays and chief rays [31]. Right combinations

Optics EXPRESS

of K_1, K_2, K_3 enable to eliminate spherical aberration, astigmatism and coma simultaneously [32]. Hence, only three parameters are needed to achieve good image quality. As a result, the remaining four design parameters, i.e., α_1, α_2, β_1 and β_2 are free. Considering big FOV is an important advantage of off-axis three-mirror systems, focal plane is set to be flat in this paper so that one more design parameter is occupied. Hence, there are three free design parameters α_1, α_2 and β_1. Once the free design parameters are determined, wave aberrations of the generated systems would be obtained and qualified automatically, and only polarization aberrations need to be calculated and optimized. Fortunately, the structural outline of three-mirror systems depends on the remaining three parameters [32], which is critical to achieve low polarization.

2.2. Automatic obscuration elimination

Removing obscuration automatically is critical to design off-axis systems. Aperture off-axis and field of view (FOV) off-axis are the two common methods to eliminate obscurations. In this paper, FOV of all systems is set to be 2°×2° whose center is at [0, -1°]. The off-axis distance of PM is used as the free variable to eliminate obscuration based on edge ray control [33]. In order to automatically judge whether there is light ray that is blocked, virtual planes are used and added in optical systems. As shown in Fig. 1, several virtual planes are built and located at the position of primary mirror (PM), secondary mirror (SM), tertiary mirror (TM) and image plane (IMG), respectively. Rays are traced at two marginal FOVs, i.e. [0°, 0°] and [0°, -2°], and two marginal apertures, i.e., +Y and -Y in the meridian plane. Obscuration is judged for all optical surfaces one by one. The surfaces that are involved at every step are shown in Table 1. In order to show the process of obscuration judgement in detail, the space from the Object to the PM is chosen as an example.

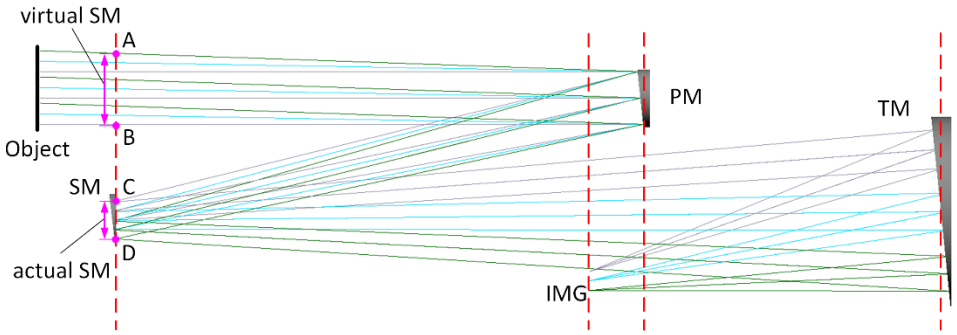

Fig. 1. Several virtual plane is used to judge obscurations.

Table 1. Virtual planes at different ranges

Number	Range	Surface
1	Object-PM	SM, IMG and TM
2	PM-SM	IMG and TM
3	SM-TM	PM and IMG
4	TM-IMG	SM and PM

The rays from the Object to the PM are traced, in which there are three virtual planes, i.e., virtual SM, virtual TM and virtual IMG. The ray parameters of all the three virtual planes are calculated. The cross section between every virtual plane and the rays is obtained and compared to the clear aperture of corresponding actual surface. For example, the coordinate of marginal

Optics EXPRESS

points A and B of cross section of the virtual SM are compared to that of points C and D from the actual SM. If obscuration exists, two conditions must be met simultaneously:

1. The virtual plane located between the Object and the PM in the direction of the optical axis;

2. There is overlapping area between AB and CD.

For the first condition, the virtual plane of the SM and that of the IMG meet while the virtual plane of the TM locates behind the PM. For the second condition, as shown in Fig. 1, the virtual planes of both the SM and the IMG do not meet. Hence, for the rays from the Object and the PM, obscuration does not exist. The above operation is repeated for the all ranges listed in Table 1. Following the above method, obviously, we can judge whether there is obscuration in the system automatically by a computer program.

During the optimization design process, however, it is found that misjudgments may occur if only the above method is used. The main reason is that real mirror is usually not a standard plane, but one with certain curvature and thickness. As shown in Fig. 2, the virtual plane of the TM is behind the PM. Hence, in our program the TM will not block the ray from the Object to the PM because the first condition is not met. However, the fact is that some rays are blocked by the upper limb of the TM because of the curvature of the TM.

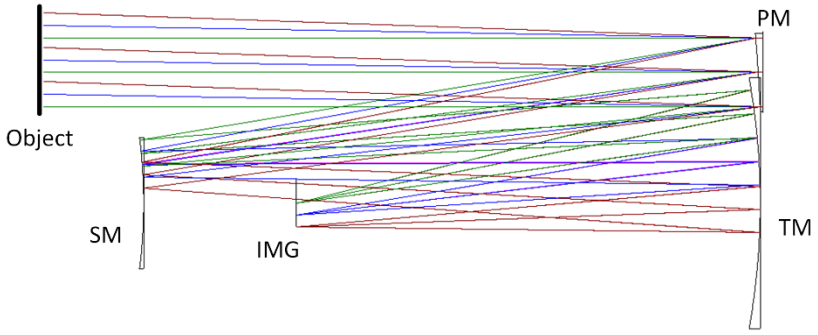

Fig. 2. A typical example to show the misjudgment about obscurations.

In order to avoid aforementioned error, four ray-quadrangles EFGH, GHJK, JKLM and LMNP are built, as shown in Fig. 3 [34]. Additional calculations are performed about obscuration between the four ray-quadrangles and the four actual surfaces, i.e., PM, SM, TM and IMG. For example, for space from the Object to the PM, edge points of the SM, TM and IMG, i.e., point J, M and N will be checked whether they locate in the ray-quadrangle EFGH. Hence, the two methods shown in Fig. 1 and Fig. 3 are combined to eliminate obscuration automatically in this paper. Misjudgments are avoided and good results are achieved. The detailed process of automatic obscuration elimination is shown in Fig. 4.

It should be noted that the target of the automatic obscuration elimination program is to find the smallest off-axis distance of a system which just enables to avoid obscuration. Obviously, larger off-axis distance can achieve obscuration elimination, too. However, larger off-axis distance results in larger polarization aberrations for the same design parameters. The detailed explanations about the relationship between polarization aberrations and off-axis distance will be provided later. Hence, for comparison purposes, off-axis distances of all systems are set to be the smallest value that just enables to eliminate obscuration. Considering the topic of this paper is to design low polarization systems, this setting is reasonable.

Optics EXPRESS

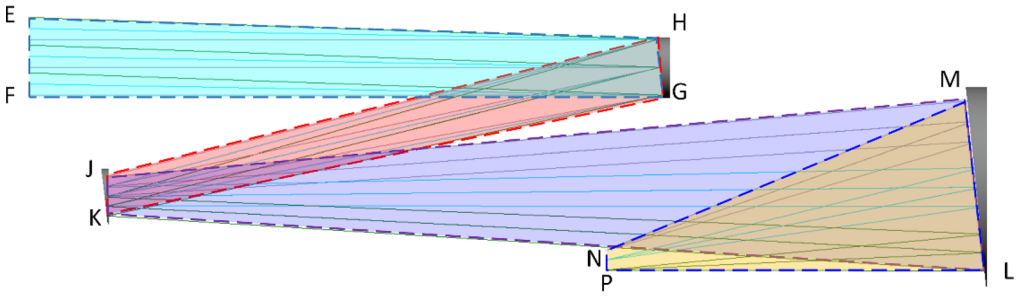

Fig. 3. The four ray-quadrangles are involved to judge obscurations.

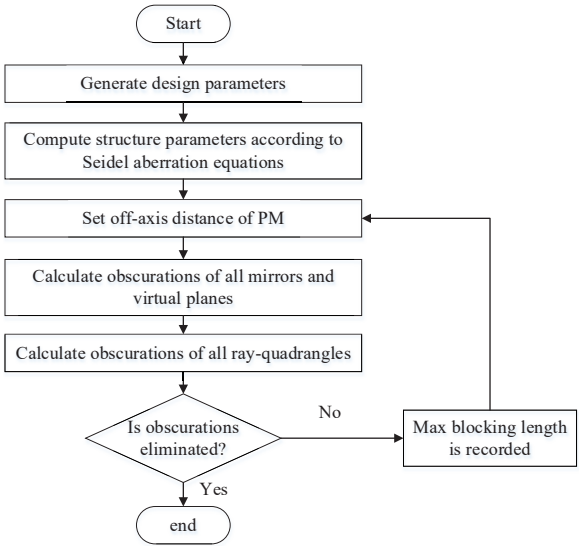

Fig. 4. The flow chart of the automatic obscuration elimination program.

2.3. *Low polarization systems design*

Genetic algorithms, which have been applied widely to find good initial configurations for optical systems [31,33,35], are used to design low polarization three-mirror systems in this paper. The flow chart of the design process is shown in Fig. 5. α_1, α_2, β_1 are chosen as the free design parameters. According to Seidel aberration equations, other four design parameters β_2, K_1, K_2 and K_3 are determined to eliminate spherical, astigmatic, coma and field curvature. Based on Eq. (1) and Eq. (2), all constructional parameters of an on-axis three-mirror system can be obtained. Then the method shown in Section 2.2 is used to eliminate obscuration in which off-axis distance of PM is set as the free variable. At this point, an off-axis three-mirror system design is completed. Wave aberrations of the system at several FOVs are recorded and polarization aberrations are calculated by three-dimensional polarization ray-tracing [18,36,37]. Hence, merit function can be built as

$$F = w_1 D + w_2 R + w_3 WFR \tag{3}$$

where D means diattenuation, R is retardance, WFR is the RMS of wave aberrations, w_i (i = 1, 2, 3) is weight factor which can be changed to adapt to different requirements. Following the basic process of genetic algorithms, different low polarization systems are designed, chosen and optimized. Finally, a local optimization for wave aberrations is performed if it is needed.

Optics EXPRESS

The local optimization is a reinforcement process for wave aberrations and is not necessary for all systems because wave aberrations of most designed systems are good enough. For a small number of systems whose wave aberrations are not completely satisfactory, tilts and decenters of both SM and TM are set as the free variables. It should be mentioned that the variations of both tilts and decenters are so small that their impacts on polarization aberrations can be ignored safely.

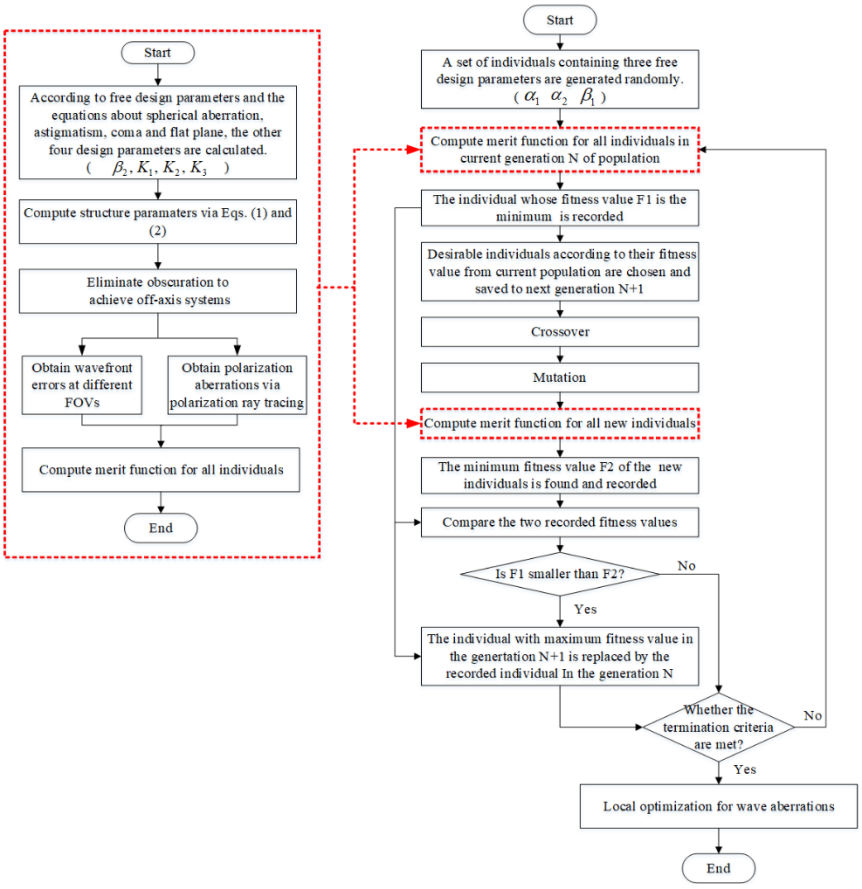

Fig. 5. The flow chart of the genetic algorithm that is used to design low polarization off-axis three-mirror optical systems.

3. Design results

In order to show the performance of the genetic algorithm in the design of low polarization off-axis three-mirror systems, some typical examples and results would be presented in this section. Firstly, an off-axis three-mirror reflective optical system that has not been optimized for low polarization will be introduced and analyzed as a reference. Then, different low polarization systems are designed in terms of different constraints and requirements via genetic algorithms. For comparison purposes, the main first-order parameters of all systems in this paper are set to be the same, as shown in Table 2. What is more, these systems are coated with barely metal aluminum, whose refraction index is 1.45 + 7.54i at 632.8 nm [38].

Optics EXPRESS

Table 2. Main first-order parameters of off-axis three-mirror systems.

Specifications	Value
Focal length/mm	1000
Entrance pupil dimeter/mm	100
The central of FOVs	[0, -1°]
FOV/°	2°×2°

3.1. Typical off-axis three-mirror reflective system

A typical off-axis three-mirror reflective system is shown in Fig. 6, whose focal length is 1000 mm and F number is 10. The free design parameters of the system are

$$[\alpha_1, \alpha_2, \beta_1] = [0.2842, 0.6137, -7.1921] \tag{4}$$

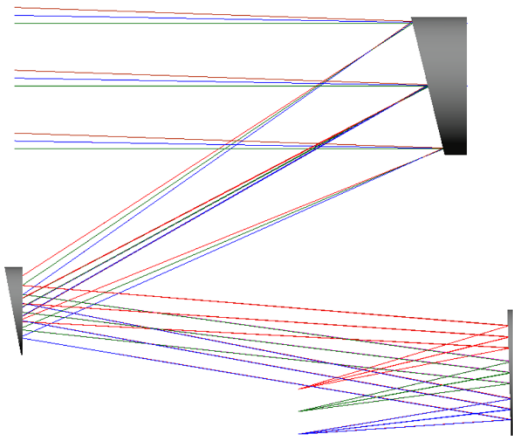

Fig. 6. Schematic diagram of a typical off-axis three-mirror reflective system.

The field curvature of the system is eliminate so that its focal plane is flat. The magnification of TM β_2 is not free and can be calculated by the third-order wave aberrations. Via the automatic obscuration elimination program shown in Section 2.2, the off-axis distance of the PM is 242 mm. The map of wave aberrations over 2°×2° field of view (FOV) is shown in Fig. 7. The average value of RMS of wave aberrations over all FOVs is 0.042λ (632.8 nm), which enables to achieve good image quality.

The polarization aberrations of the off-axis three-mirror system are analyzed. Cumulative diattenuation and retardance of rays going through all the three mirrors are obtained by three-dimensional polarization ray-tracing. The FOV of the system is 2°×2°. Polarization aberrations are related to FOVs. At every aperture position, the system at 25 different FOVs is analyzed. The distribution of these FOVs is shown in Fig. 8. Polarization aberrations at every aperture position are the corresponding average value over the 25 FOVs. Results are shown in Fig. 9(a) and (b), respectively, in which polarization aberrations distribute at different aperture positions in the entrance pupil plane of the system. It can be seen that both the diattenuation map and retardance map are non-rotationally symmetric, which have been analyzed in detail in our previous paper [19]. The maximum diattenuation is 0.0129 and the maximum retardance is 0.0674 rad, which appear at the area away from the optical axis. In order to compare polarization aberrations in different systems, the polarization aberrations along different aperture positions at one azimuth angle are picked out and compared, as shown as the red dot line in Fig. 9. Diattenuation in the

Optics EXPRESS

red dot line in Fig. 9(a) is shown as the orange-square curves in Fig. 10(a). Retardance is shown in Fig. 10(b).

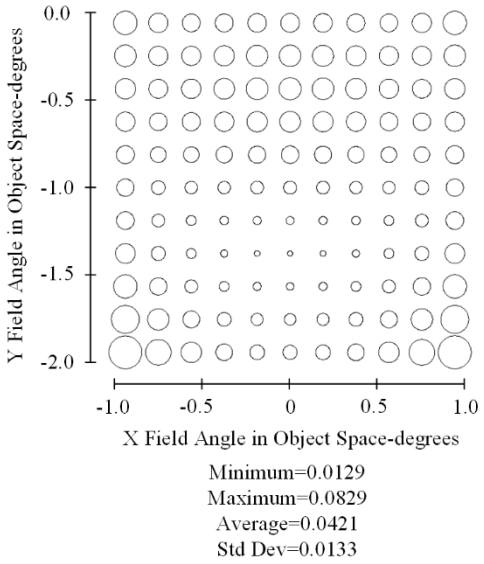

Fig. 7. RMS of wave aberrations vs field angle in object space of the normal system.

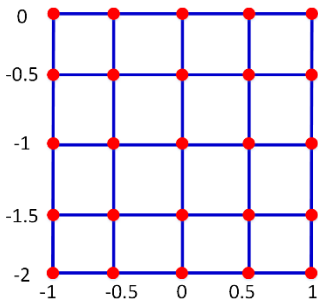

Fig. 8. The distribution of 25 FOVs involved in the calculation.

3.2. Example 1

Let us start low polarization off-axis three-mirror reflective systems design by the genetic algorithm. The merit function is shown as Eq. (3). Both polarization aberrations and wave aberrations are involved. One typical result is shown in Fig. 11, whose free design parameters are

$$[\alpha_1, \alpha_2, \beta_1] = [0.3431\ 0.8871\ -\ 14.9715]. \tag{5}$$

Via the automatic obscuration elimination program shown in Section 2.2, the off-axis distance of PM is 120 mm. As shown in Fig. 11, obscuration is avoided with small gaps, which is the result of our automatic obscuration elimination program shown in Sec 2.2. The merit function variation verus evloving generations is shown in Fig. 12. The wave aberrations of the system over 2°×2° FOVs are shown in Fig. 13. The average of RMS of wave aberrations is only 0.00855 λ (632.8 nm). Obviously, good image quality can be achieved. Cumulative polarization

Optics EXPRESS

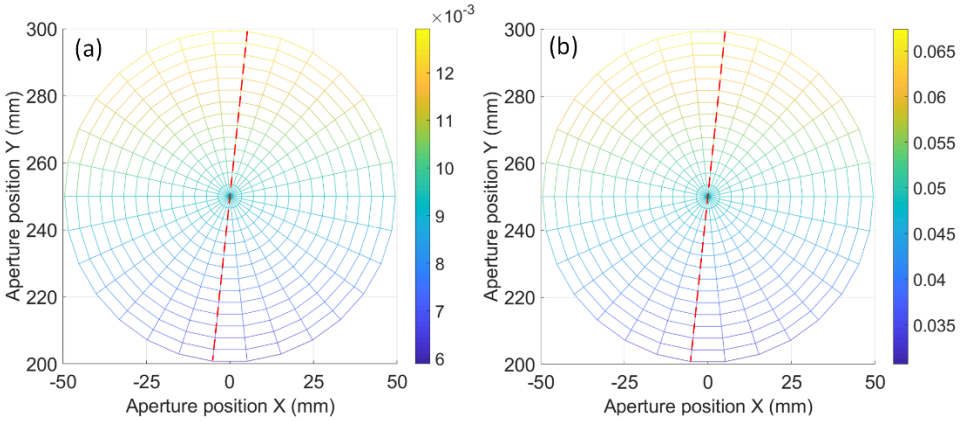

Fig. 9. Cumulative (a) diattenuation (dimensionless) map and (b) retardance (radians) map over the entrance pupil plane.

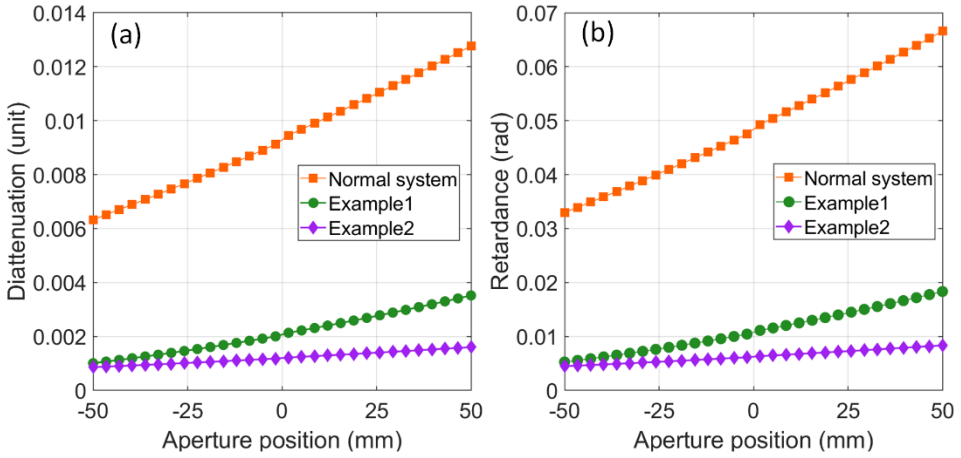

Fig. 10. (a) Diattenuation and (b) retardance along different aperture positions at one azimuth angle.

aberrations of the system are calculated. Diattenuation and retardance of the system are compared to the counterparts of the normal system shown in Fig. 6, respectively. Results are shown as the green-circular curves in Figs. 10(a) and (b). It can be seen that polarization aberrations of the system in Fig. 11 are drastically reduced after low polarization design. The maximum diattenuation is reduced from 0.0129 to 0.0038. The maximum retardance is reduced from 0.067 to 0.018, respectively. The polarization aberrations of the example 1 are about only one-third of the normal system.

3.3. *Example 2*

It is found that the ranges of free design parameters have impacts on final design results. In the example 1, both α_1 and α_2 are positive while β_1 is negative. If all the three design parameters are positive, different results can be obtained. An example is shown in Fig. 14, whose free design parameters are

$$[\alpha_1, \alpha_2, \beta_1] = [0.3922\ 1.8576\ 2.66]. \tag{6}$$

Optics EXPRESS

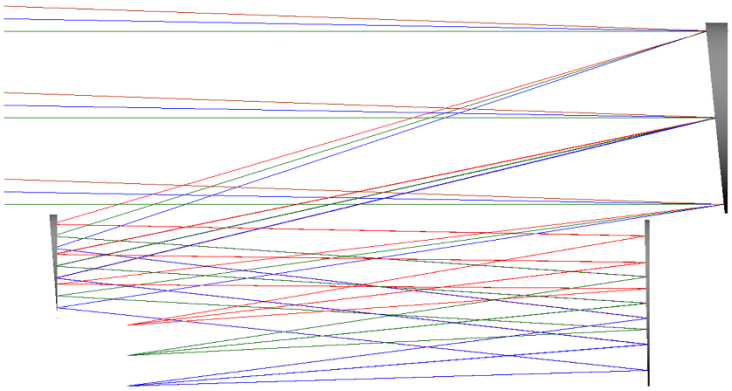

Fig. 11. Schematic diagram of the example 1.

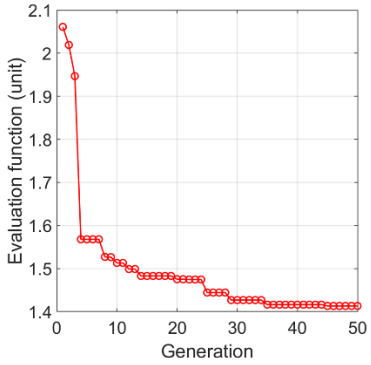

Fig. 12. Merit function variation curve.

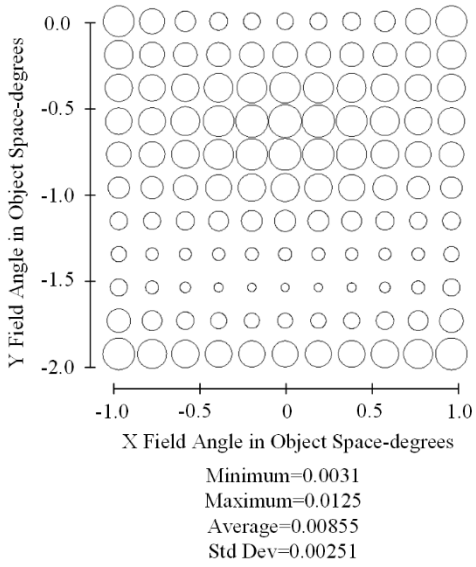

Fig. 13. RMS of wave aberrations vs field angle in object space of the example 1.

Optics EXPRESS

Via the automatic obscuration elimination program shown in Section 2.2, the off-axis distance of PM is 250 mm. The wave aberrations of the system over 2°×2° FOVs are shown in Fig. 15. The average of RMS of wave aberrations is 0.0417 λ (632.8 nm). Cumulative polarization aberrations of the system are calculated. Results are shown as the purple-diamond curves in Figs. 10(a) and (b). It can be seen that polarization aberrations of the system in Fig. 14 are further smaller than those of example 1. However, the aperture of the TM in example 2 is larger than that of the PM, which may become a disadvantage in engineering applications.

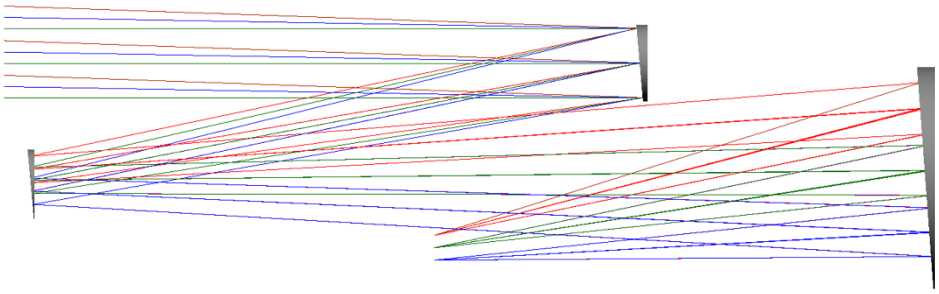

Fig. 14. Schematic diagram of example 2.

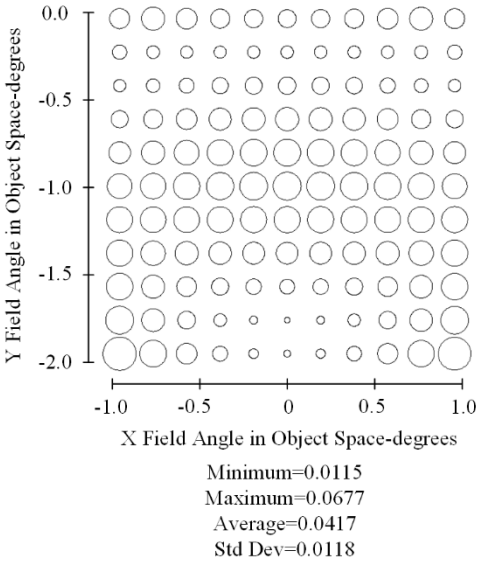

Fig. 15. RMS of wave aberrations vs field angle in object space of example 2.

4. Relationship between off-axis distance and polarization aberrations

In low polarization off-axis systems design process, it is found that polarization aberrations are very relevant to off-axis distances of PM. In Fig. 16(a), there are 50 populations that have been optimized for low polarization aberrations by the genetic algorithm. Off-axis distances and corresponding polarization aberrations of all the populations are plotted together. It can be seen that the off-axis distances are almost synchronous to the polarization aberrations in Fig. 16(a). The 50 populations are sorted based on off-axis distances and shown in Fig. 16(b). For most populations, polarization aberrations decrease gradually, as well as the off-axis distances.

Optics EXPRESS

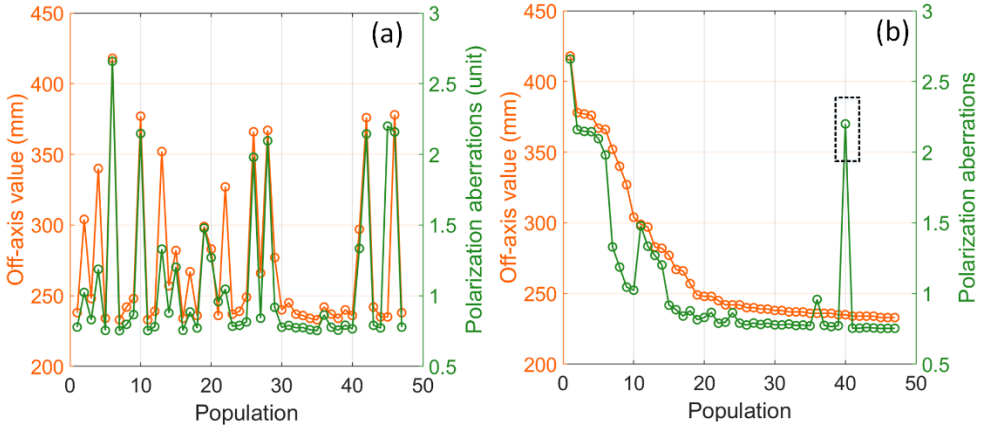

Fig. 16. The relationship between off-axis distances and polarization aberrations. (a) 50 populations that have been optimized for low polarization aberrations design. (b) The 50 populations are sorted according to off-axis distances.

In fact, it is easy to understand the relationship between off-axis distances and polarization aberrations shown in Figs. 16(a) and (b). For an off-axis optical system whose constructional parameters such as surface curvatures, conic constants and separations are determined, bigger off-axis distances mean bigger incident angles. According to Fresnel equations, polarization aberrations are dependent on angle of incidence if refractive index of mirrors is chosen. In most cases, hence, systems with bigger off-axis distances have higher polarization aberrations. In order to minimize polarization aberrations as much as possible, off-axis distances of all the systems in this paper are set to be the smallest values that just enable to eliminate obscurations. Obviously, systems whose obscurations can be eliminated by small off-axis distances probably have important advantages in low polarization design. In practical engineering applications, of course, there are often other factors such as structural design should be also considered when off-axis distance of PM of a system is chosen and determined.

However, there are also some exceptions. It can be seen in Fig. 16(b) that there is a system circled by a black dotted line. It is picked out and shown in Fig. 17(a). The system is named as example 3. The free design parameters of example 3 are

$$[\alpha_1, \alpha_2, \beta_1] = [0.3947\ 1.2575\ 13.6902], \tag{7}$$

whose off-axis distance of PM is 235 mm. To compare with example 3, another system whose off-axis distance of PM is 245 mm is shown in Fig. 17(b). The system is named as example 4. Design parameters of example 4 are

$$[\alpha_1, \alpha_2, \beta_1] = [0.3922\ 1.8576\ 2.6600]. \tag{8}$$

Design parameters of both the two systems are positive. The diattenuation and retardance of the two systems are shown in Fig. 18(a) and (b), respectively. Although off-axis distance is increased by 10 mm, polarization aberrations of example 4 are about only one-third of those of example 3.

The reasons for the abnormal relationship between polarization aberrations and off-axis distances in example 3 and example 4 are analyzed. According to Eq. (7) and Eq. (8), β_1 of the example 3 is 13.6902 and is far bigger than that of example 4. β_1 means longitudinal magnification of secondary mirror. According to Eq. (1), bigger β_1 generate smaller r_1 and r_2. The radii of mirrors in the two examples are shown in Table 3. It can be seen that the radii of

Optics EXPRESS

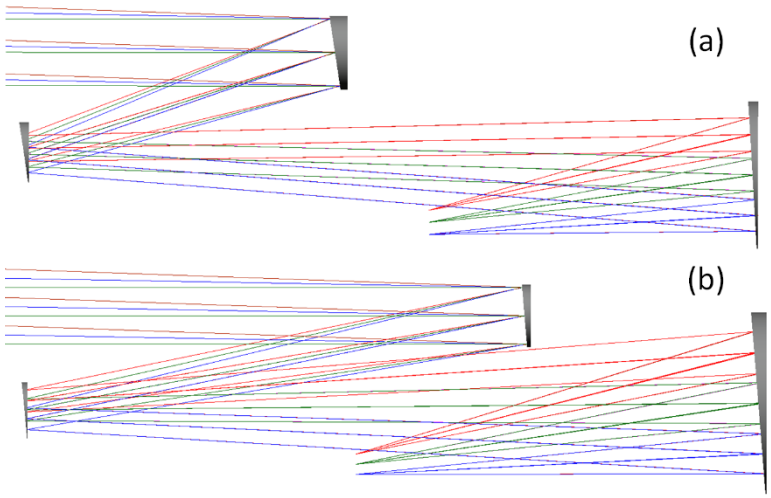

Fig. 17. Two off-axis three-mirror systems. (a) The example 3 whose off-axis distance is 235 mm and (b) example 4 whose off-axis distance is 245 mm.

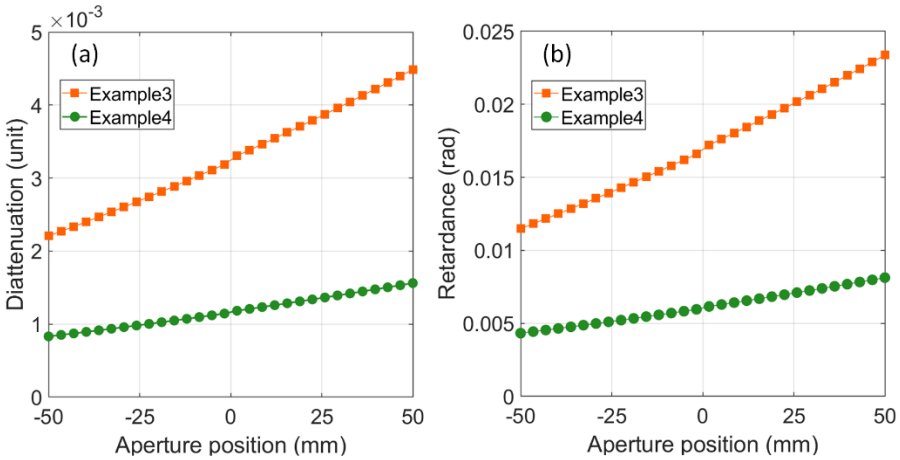

Fig. 18. (a) Diattenuation and (b) retardance along different aperture positions at one azimuth angle.

all mirrors in the example 3 are smaller than the corresponding values in the example 4. As a result, the incident angle probably be larger when a light ray is reflected by the optical surfaces with smaller curvature radii. Hence, polarization aberrations become larger. This is the primary reason why polarization aberrations of the two systems shown in Fig. 17 are different.

Table 3. The radii of example 3 and example 4

	Example 3	Example 4
r_1 (mm)	-1559.9477	-2902.9106
r_2 (mm)	-573.7983	-827.4501
r_3 (mm)	-907.667	-1157.3401

Optics EXPRESS

However, it should be emphasized that radii of mirrors can not be used as the merit function to design low polarization systems although calculations are simpler because polarization ray tracing can be avoided. If radii of all the three mirrors are smaller, polarization aberrations indeed are lower. However, the relationship between radii of three mirrors is usually complex, such as r_1 is bigger while r_2 is smaller. It becomes difficult to determine which system has smaller polarization aberrations. More detailed analyses about this can be found in our previous paper [18]. According to the above comparisons and analyses, it can be found that polarization aberrations of off-axis three-mirror systems are complicated and dependent on several factors, such radii of all mirrors, off-axis distances, and so on. Hence, polarization aberrations are the most suitable merit function to design low polarization systems although calculations would be more complex and time-consuming.

5. Conclusions

Off-axis optical systems have several important advantages over on-axis ones. However, high polarization aberrations become a critical disadvantage of off-axis systems. It would be desirable if off-axis systems are designed to be with low polarization aberrations. In this paper, a method based on genetic algorithms is proposed to design off-axis three-mirror systems with good wave aberrations and low polarization aberrations. There are seven free design parameters in three-mirror optical systems. For most imaging applications, wave aberrations are far more important than polarization aberrations. Hence, four of them are used to eliminate the primary third-order wave aberrations and achieve flat image plane. The remaining three parameters are free and can be used to optimize and reduce polarization aberrations.

Obscuration elimination and optimizing polarization aberrations are the two main steps to design off-axis three-mirror systems with low polarization aberrations. An automatic obscuration elimination program is developed. Off-axis distance of PM is used as the free variable to eliminate obscuration based on edge ray control. In order to automatically judge whether there is light ray that is blocked, both virtual planes and ray-quadrangles are involved. Accurate judgments about obscurations are achieved successfully. To minimize polarization aberrations as much as possible, off-axis distances of all the systems in this paper are set to be the smallest values that just enable to eliminate obscurations.

Genetic algorithms are used to optimize polarization aberrations. Both wave aberrations and polarization aberrations are concluded into the merit function. Typical design results are provided. After low polarization design, the average of RMS of wave aberrations over 2°×2° FOVs is 0.00855 λ (632.8 nm), which is enough for the system to achieve good image quality. The maximum diattenuation is reduced from 0.0129 to 0.0038. The maximum retardance is reduced from 0.067 to 0.018. Obviously, polarization aberrations have been reduced to one-third of its original value. During low polarization off-axis systems design process, it is found that polarization aberrations are very relevant to off-axis distances. In most cases, systems with bigger off-axis distances have higher polarization aberrations. For low polarization applications, hence, off-axis distances should be set to be the smallest values that just enable to eliminate obscurations if other factors such as structural design allow. Additionally, systems whose obscurations can be eliminated by small off-axis distances probably have important advantages in low polarization design. The method proposed in this paper is universal and can be used widely to design other types of optical systems that demand low polarization.

Funding. National Natural Science Foundation of China (12003033); Youth Innovation Promotion Association of the Chinese Academy of Sciences (2023225); National Key Research and Development Program of China (2021YFC2802100).

Acknowledgment. We thank Synopsys for the educational license of CODE V.

Disclosures. The authors declare no conflicts of interest.

Optics EXPRESS

Data availability. Data underlying the results presented in this paper are not publicly available at this time but may be obtained from the authors upon reasonable request.

References

1. D. Korsch, "Design and optimization technique for three-mirror telescopes," Appl. Opt. **19**(21), 3640–3645 (1980).
2. L. G. Cook, "Three-mirror anastigmat used off-axis in aperture and field," Proc. SPIE **0183**, 207–211 (1979).
3. G R. Laureijs, J. Amiaux, and S. Arduini, *et al.*, "Euclid definition study report," arXiv, arXiv:1110.3193 (2011).
4. J. B. Hadaway, D. M. Chaney, and L. B. Carey, "The optical metrology system for cryogenic testing of the JWST primary mirror segments," Proc. SPIE **8126**, 50–58 (2011).
5. Y. Gong, X. W. Liu, and Y. Cao, *et al.*, "Cosmology from the Chinese Space Station Optical Survey (CSS-OS)," Astrophys. J. **883**(2), 203 (2019).
6. D. M. Harrington and S. R. Sueoka, "Polarization modeling and predictions for Daniel K. Inouye Solar Telescope part 1: telescope and example instrument configurations," J. Astron. Telesc. Instrum. Syst. **3**(1), 018002 (2017).
7. D. John, R. Mill, and R. O'Neil, *et al.*, "Midcourse space experiment: introduction to the spacecraft, instruments, and scientific objectives," J. Spacecr. Rockets **31**(5), 900–907 (1994).
8. X. Bai, B. Xu, and H. Ma, *et al.*, "Aberration fields of pupil-offset off-axis two-mirror astronomical telescopes induced by ROC error," Opt. Express **28**(21), 30447–30465 (2020).
9. B. Sang, J. Schubert, and S. Kaiser, *et al.*, "The EnMAP hyperspectral imaging spectrometer: instrument concept, calibration, and technologies," Proc. SPIE **7086**, 708605 (2008).
10. R. A. Chipman, G. Young, and W. S. T. Lam, Polarized Light and Optical Systems (CRC press, 2018), Chap. 15.
11. J. Ruoff and M. Totzeck, "Orientation Zernike polynomials: a useful way to describe the polarization effects of optical imaging systems," J. Micro/Nanolithogr., MEMS, MOEMS **8**(3), 031404 (2009).
12. J. Luo, D. Liu, and Z. Huang, *et al.*, "Polarization properties of receiving telescopes in atmospheric remote sensing polarization lidars," Appl. Opt. **56**(24), 6837–6845 (2017).
13. J. Luo, X. He, and K. Fan, *et al.*, "Effects of polarization aberrations in an unobscured off-axis space telescope on its PSF ellipticity," Opt. Express **28**(25), 37958–37970 (2020).
14. F. C. M. Bettonvil, M. Collados, and A. Feller, *et al.*, "The polarization optics for the European Solar Telescope (EST)," Proc. SPIE **7735**, 77356I (2010).
15. A. J. Brown, T. I. Michaels, and S. Byrne, *et al.*, "The case for a modern multiwavelength, polarization-sensitive LIDAR in orbit around Mars," J. Quant. Spectrosc. Radiat. Transfer **153**, 131–143 (2015).
16. R. M. Anche, J. N. Ashcraft, and S. Y. Haffert, *et al.*, "Polarization aberrations in next-generation giant segmented mirror telescopes (GSMTs) I. Effect on the coronagraphic performance," arXiv, arXiv:2304.02079 (2023).
17. S. D. Will and J. R. Fienup, "Effects and mitigation of polarization aberrations in LUVOIR coronagraph," Proc. SPIE **11117**, 1111710 (2019).
18. J. Luo, T. Xu, and X. He, *et al.*, "Low polarization on-axis three-mirror reflective optical systems initial configuration designed by genetic algorithms," Opt. Commun. **528**, 129053 (2023).
19. J. Luo, C. You, and X. He, *et al.*, "Comparisons between an on-axis three-mirror anastigmat telescope and an off-axis one: polarization aberrations," Appl. Opt. **60**(22), 6438–6447 (2021).
20. F. Zeng, X. Zhang, and J. Zhang, *et al.*, "Optics ellipticity performance of an unobscured off-axis space telescope," Opt. Express **22**(21), 25277–25285 (2014).
21. B. Singaravelu and R. A. Cabanac, "Obstructed telescopes versus unobstructed telescopes for wide field survey—a quantitative analysis," Publ. Astron. Soc. Pac. **126**(938), 386–397 (2014).
22. J. Kuhn and S. Hawley, "Some astronomical performance advantages of off-axis telescopes," Publ. Astron. Soc. Pac. **111**(759), 601–620 (1999).
23. J. Davis, M. K. Kupinski, and R. A. Chipman, *et al.*, "HabEx polarization ray trace and aberration analysis," Proc. SPIE **10698**, 106983H (2018).
24. A. Boccaletti, J. Schneider, and W. Traub, *et al.*, "SPICES: spectro-polarimetric imaging and characterization of exoplanetary systems from planetary disks to nearby Super Earths," Exp. Astron. **34**(2), 355–384 (2012).
25. M. E. Levi, M. Lampton, and A. G. Kim, *et al.*, "Science yield of an improved Wide Field Infrared Survey Telescope (WFIRST)," arXiv, arXiv:1105.0959 (2011).
26. Q. Meng, D. Wang, and X. Wang, *et al.*, "High Resolution Imaging Camera (HiRIC) on China's first Mars exploration Tianwen-1 mission," Space Sci. Rev. **217**(3), 42 (2021).
27. T. R. Rimmele, M. Warner, and S. L. Keil, *et al.*, "The Daniel K. Inouye Solar Telescope – observatory overview," Sol. Phys. **295**(12), 172 (2020).
28. S. Keil, T. Rimmele, and C. Keller, "Design and development of the advanced technology solar telescope," Astron. Nachr. **324**(4), 303–304 (2003).
29. J. Breckinridge, M. Kupinski, and J. Davis, *et al.*, "Terrestrial exoplanet coronagraph image quality: study of polarization aberrations in Habex and LUVOIR update," Proc. SPIE **10698**, 106981D (2018).
30. M. R. Bolcar, "LUVOIR telescope design overview," (2016).
31. L. Jun, W. Huang, and F. Hongjie, "A novel method for finding the initial structure parameters of optical systems via a genetic algorithm," Opt. Commun. **361**, 28–35 (2016).
32. J. Pan, *The Design, Manufacture and Test of the Aspherical Optical Surfaces* (Suzhou University Press, 2004), Chap. 5.

Optics EXPRESS

33. Z. Mi, Z. Li, and X. Zhang, "Construction of a compact off-axis three-mirror reflective system," Appl. Opt. **61**(9), 2424–2431 (2022).
34. C. Xu, D. Cheng, and Y. Wang, "Automatic obscuration elimination for off-axis mirror systems," Appl. Opt. **56**(32), 9014–9022 (2017).
35. K. Höschel and V. Lakshminarayanan, "Genetic algorithms for lens design: a review," J. Opt. **48**(1), 134–144 (2019).
36. G. Yun, K. Crabtree, and R. A. Chipman, "Three-dimensional polarization ray-tracing calculus I: definition and diattenuation," Appl. Opt. **50**(18), 2855–2865 (2011).
37. G. Yun, S. C. McClain, and R. A. Chipman, "Three-dimensional polarization ray-tracing calculus II: retardance," Appl. Opt. **50**(18), 2866–2874 (2011).
38. D. Raki and Aleksandar, "Algorithm for the determination of intrinsic optical constants of metal films: application to aluminum," Appl. Opt. **34**(22), 4755–4767 (1995).